

Copyright
by
Rose Janet Simmons
2017

The Report committee for Rose Janet Simmons
Certifies that this is the approved version of the following report:

Methods for Kinematic Analysis of the Right Ventricle

APPROVED BY

SUPERVISING COMMITTEE:

Michael Sacks, Supervisor

Reza Avazmohammadi

Methods for Kinematic Analysis of the Right Ventricle

by

Rose Janet Simmons, B.S.C.S.

REPORT

Presented to the Faculty of the Graduate School of

The University of Texas at Austin

in Partial Fulfillment

of the Requirements

for the Degree of

Master of Science in Computational Science, Engineering and Mathematics

THE UNIVERSITY OF TEXAS AT AUSTIN

May 2017

Dedicated to my grandmother.

Acknowledgments

I would like to thank the following people for contributing to this report:

- My committee members: Michael Sacks, PhD for supervising this report and sparking my interest in cardiac modeling. Reza Avazmohammadi, PhD for serving as a reader for my report.
- Karen Tsai, M.S. and Devesh Sahu, M.S. for their previous work on this project and providing pipeline images.
- All other researchers, students and research groups involved in this ongoing project including: Ronald Peshock, M.D., The Institute for Computational Engineering and Sciences (ICES), The Center for Cardiovascular Simulation, UT Southwestern Medical Center
- My friends and family for encouraging me during every step of my education.

Methods for Kinematic Analysis of the Right Ventricle

Rose Janet Simmons, M.S.C.S.E.M.
The University of Texas at Austin, 2017

Supervisor: Michael Sacks

Despite playing a large role in many cardiovascular diseases (such as pulmonary hypertension), the heart's right ventricle (RV) is still poorly understood in regards to its complex shape and motion over the cardiac cycle. In this report, we examine the kinematics of the right ventricle and our ongoing progress towards developing a computational pipeline to extract functional measurements of deformation from cardiac computed tomography (CT) images. While other techniques in [2], [9], and [31] have been used to model the RV shape and motion, they lack a clear physical interpretation of their results. By using a central axis governed by blood flow direction, left ventricle based coordinate system, and deformable NURBS shape representation, we aim to identify kinematic modes that have a more direct physiological meaning. In doing so, the proposed methods could be eventually developed into an image-based tool for both diagnostic and prognostic purposes.

Table of Contents

Acknowledgments	v
Abstract	vi
List of Tables	ix
List of Figures	x
Chapter 1. Introduction	1
Chapter 2. Overview of the Right Ventricle	3
2.1 Structure	3
2.2 Comparison to Left Ventricle	4
2.3 Pathology	6
2.4 Kinematics	7
Chapter 3. Previous Methods	8
3.1 Spherical Harmonic Mapping [32]	8
3.2 Tagged MRI [10]	9
3.3 Shape Representation using NURBS [3]	10
Chapter 4. Data Processing Pipeline	12
4.1 Clinical Data	13
4.2 Determining End Planes	13
4.3 Determining the Central Axis	14
4.3.1 Sectional Centroids	15
4.3.2 Second Bezier Curve	17
4.4 Remapping	19

Chapter 5. Preliminary Deformation Analysis	21
5.1 NURBS	21
5.1.1 Definition	22
5.1.2 Deformation	24
5.2 Application	25
Chapter 6. Conclusion and Future Work	27
Bibliography	29
Vita	34

List of Tables

5.1	Relative axes length over the five phase points for one normal RV.....	26
-----	--	----

List of Figures

2.1	Anatomy and blood flow of the heart.	4
2.2	Relative thickness and shape of the left and right ventricles. . .	5
2.3	Normal left ventricle (LV) and right ventricle (RV) pressure-volume relationships. Image from [30].	7
4.1	Data processing pipeline for analyzing cardiac CT images . . .	12
4.2	The two best-fit end planes and their respective normal vectors.	14
4.3	Bezier curve and its control points alongside the point cloud $P(x, y, z)$. Parameter values of a=65 and b=59 were used. . .	16
4.4	The right ventricle point cloud with the initial bezier curve (purple), the sectional centroids (green), and two end normals (yellow)	17
4.5	Central axis and sectional centroids (and corresponding sectional planes).	18
4.6	The re-mapped point clouds with the central axis shown in green.	20
5.1	The two main methods of modifying a NURBS curve. (a) The effect of displacing control point p_k to p_k^* along direction v by a distance d . This produces a new curve $p^*(u)$ which is partially shifted towards v . (b) The result of assigning a new weight w_k^* to the k -th control point. The origin O of the coordinate system is set to control point p_k . Images from [27].	24
5.2	The re-mapped point clouds over time from three perspectives.	25
5.3	Four main types of motion expected to make up RV kinematics. (1) Elongation and contraction. (2) Twisting and rinsing. (3) Peristaltic movement. (4) Bending.	26

Chapter 1

Introduction

Among doctors and philosophers alike, the heart is considered to be one of the most complex and important organs in the human body and has been studied by the likes of Aristotle, Galen, and Leonardo Da Vinci. In modern times, understanding cardiology has become even more crucial as cardiovascular disease has become the number one cause of death by far [1]. With a clear need for advancements in both early diagnosis and treatment, cardiac modeling has emerged as a vital tool for analyzing medical imaging data and simulating cardiac function. Despite these decades of research, the right ventricle specifically is still poorly understood in comparison to its left counterpart. As we now know, it plays a large role in cardiac disease and dysfunction which creates a clear need for further study of the right ventricle. As shown throughout this paper, this presents unique challenges and requires creative computational techniques.

In this report, we will give an overview of the structure and kinematics of the right ventricle as a motivation for using deformable geometric models to characterize its shape and movement across the cardiac cycle. Chapter 2 will point out some of the important biological and mechanical features of the right

ventricle and the role of disease. In Chapter 3, some related geometric and kinematic models will be reviewed to preface the our choice of computational techniques. Finally, Chapters 4 and 5 detail the novel methods and analysis of our ongoing project by the Center for Cardiovascular Simulation at UT Austin to create a thorough computational framework for kinematic analysis of right ventricle images.

Further, we will discuss how these techniques have the potential to be extended for comparison between subjects with and without diseases such as pulmonary hypertension. With this information in hand, we hope to better describe the contractile dynamics in the RV and predict how cardiovascular disease affects its behavior. This could provide crucial information that could be applied towards the ultimate goal of more clinical tools for prognosis and diagnosis of diseases affecting the right ventricle.

Chapter 2

Overview of the Right Ventricle

While many strides have been made in the field of cardiac modeling, the majority of the efforts have been applied to the left ventricle (LV) of the heart. In this section, we briefly explore some of the main functional and structural characteristics that are unique to the right ventricle (and which can also make it difficult to study).

2.1 Structure

To maintain the complex cardiac cycle, the heart must manage a precisely-timed chain of mechanical and electrical events with little to no room for error. In order to do so, the heart's anatomy is divided into four main chambers with a ventricle and atrium on each respective side as shown in Figure 2.1. Within this system, the right ventricle's function is to receive de-oxygenated blood from the right atrium above and then push it out to the pulmonary artery where it can be transported to the lungs for oxygenation [10]. The right ventricle itself is situated below the right atrium and directly opposite to the left ventricle. The septum divides the two ventricles and is their shared structural wall while the opposing wall is referred to as the right ventricle free wall

(RVFW). The RV anatomy can be subdivided into three main components: the inlet, apical trabecular and the outlet as described by Goor and Lillehei [8]. This can be more simply put as the sinus (for inflow) and conus (for out-flow) but does not allow for as much distinction between the morphology of the two ventricles [12].

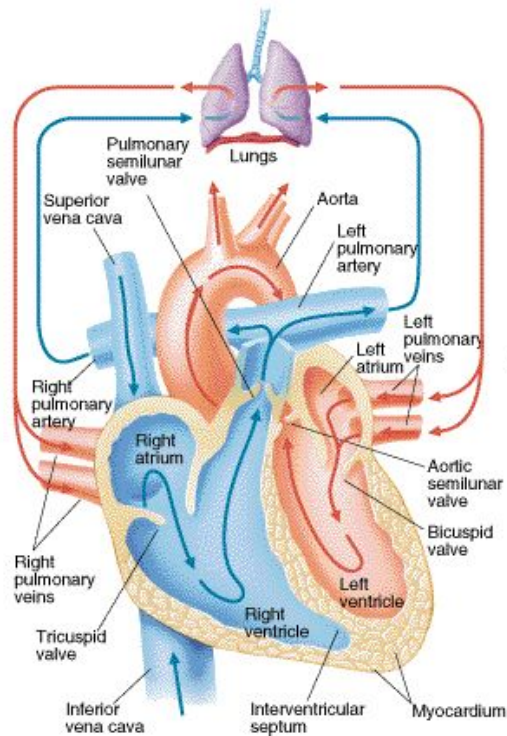


Figure 2.1: Anatomy and blood flow of the heart.

2.2 Comparison to Left Ventricle

The left ventricle had long been attributed to being more responsible for (and affected by) cardiovascular diseases and other sources of hypertrophy.

Early experiments observed that cardiac output was mainly unaffected when the right ventricle free wall (RVFW) was ablated or replaced and was therefore considered to be non essential in comparison [30]. However, it has been since shown that the failure of the right ventricle is in fact a key determinant of morbidity and mortality in pulmonary hypertension [15].

As shown below in Figure 2.2, we can also clearly see that the two ventricles are quite structurally asymmetric. The right ventricle wraps around the ellipsoidal left ventricle to form a irregular crescent-like shape in a cross-section [11] which is not as ideal for many geometric representations. The left ventricle's free wall is also two to three times thicker than that of the right ventricle [13]. Further, while the right ventricle is larger than the LV in terms of volume, it is only about one-sixth of the LV mass [17]. Due to this, the RV has a higher surface-to-volume ratio and requires a smaller contraction to achieve the same stroke volume [11].

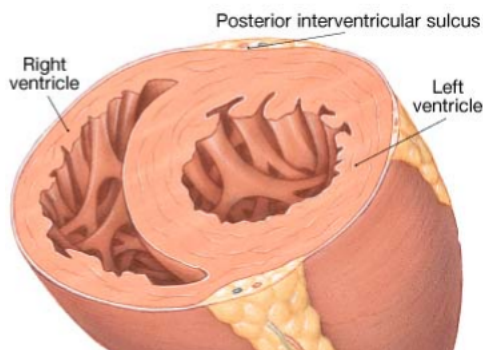


Figure 2.2: Relative thickness and shape of the left and right ventricles.

2.3 Pathology

The cardiovascular system is interconnected to almost every aspect of human health so it is no surprise that even acute or minor conditions of a single ventricle of the heart can have lasting effects on a patient. When there is ventricular dysfunction, it can often lead to adaptive remodeling of the muscle and movement in the heart [24]. While this initially seems like a positive mechanism, this also means that RV dysfunction (and failure) can often lack clinical symptoms or manifest itself by instead affecting the LV or lungs.

A particular example of this is pulmonary hypertension (PH), which is a progressive condition characterized by elevated pressure in the pulmonary artery which can lead to hypertrophy and increased resistance in the lungs [24][21]. Not only does it lead to over 300,000 hospitalizations annually, but its frequency and mortality rates have shown period of significant increases in the last couple decades in the U.S. [7]. In terms of right ventricle analysis, PH is of particular significance because the RV function is the important indicator of both prognosis and diagnosis of PH [21]. In one particular study, more than half of the deaths of patients with PH were ultimately attributed to right heart failure [5]. In terms of research, however, the strong attachment to RV function, frequent occurrence, and overwhelmingly negative outlook makes it an ideal disease to study as improvement can have a tangible impact.

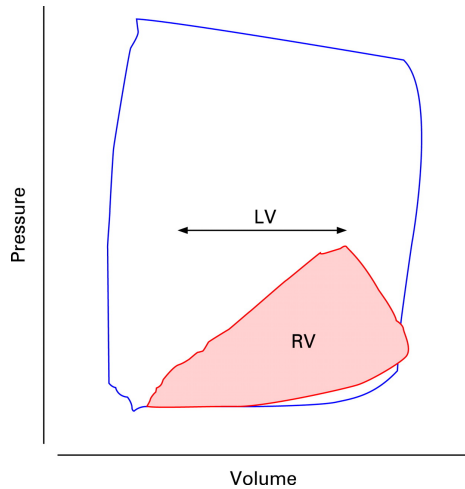


Figure 2.3: Normal left ventricle (LV) and right ventricle (RV) pressure-volume relationships. Image from [30].

2.4 Kinematics

As an organ that is in continuous motion, the heart has a dynamic geometry with the RV having especially complex motion. During ventricular systole, the right ventricle contracts to push blood through the pulmonary artery to be oxygenated as its primary function. The contraction mechanism causes the free wall to move inward towards the center and shortens the long axis due to contraction of its longitudinal fibers [31]. Once the ventricles relax in diastole, the tricuspid valve (between the right atrium and right ventricle) opens and the ventricular fibers relax as it expands and once again fills with blood in order to repeat the next cycle [29]. As displayed in Fig. 2.3, it is also clear that the pressure-volume profiles of each is vastly different with the RV having poorly defined isovolumic periods and sustained ejection even during pressure decline [29].

Chapter 3

Previous Methods

There are many methods to model and characterize biological systems in terms of their geometric and mechanical qualities. In this section, we briefly examine some previous techniques applied to cardiac modeling including relevant results or drawbacks. Additionally, we introduce using NURBS as a representation for geometric data and why it is well suited for this problem.

3.1 Spherical Harmonic Mapping [32]

One particularly relevant project in recent years was done by Wu et al in 2012 which introduced a new approach to fit the RV endocardial surface using spherical harmonics [32]. With a similar motivation, their study examined cardiac CT images of the right ventricle throughout the cardiac cycle in order to improve understanding of changes due to pulmonary hypertension. After manually segmenting the CT images, analytical 3-D meshes were generated and then smoothed using a discrete Gaussian filter. For the surface parameterization, each endocardial surface at time point t is mapped to a reference state using a variation of two-step harmonic topological mapping. By first applying a harmonic mapping (in which each new parameter satisfies Laplace's

equation), and then a secondary mapping (to improve surface distribution) images of the heart across time can be analyzed in anatomically consistent manner [32]. This deterministic approach creates a unique, one-to-one mapping between the original mesh and unit sphere. In order to analyze the surface, they created "pseudo-displacement" function based on the normalized shape change over time for an individual and then used proper orthogonal decomposition (POD) to rank a set of kinematic features/modes amongst a group of individuals[32]. While the pipeline is mathematically robust with promising results, the main issue with their approach is the lack of clear physiological meaning of the psuedo-displacement functions and computed kinematic modes. Further, this means the results are highly dependent on the initial reference points used in the mapping.

3.2 Tagged MRI [10]

In another paper from Haber et al in 2000, tagged multi-view magnetic resonance imaging (MRI) data was used to reconstruct and visualize right ventricular motion in three dimensions [10]. In order to accurately include the function of the intra-ventricular septum, they decided to use a bi-ventricular model and implemented it as a finite element mesh built from segmented contours. These contours were automatically generated via SPAMMVU which uses spatial modulation of magnetization to track the tags across the images. To reconstruct the motion, a deformable model was used by energy minimization in terms of a reduced form of Lagrange's equation which relates the

deformation and finite element stiffness. One potential difficulty of the tagging method is the relatively large distance between tags (6mm apart) limits the amount that can be positioned on the RV free wall to capture information. In this project, the work was primarily focused on the methodology of their approach rather than a particular disease, but applied it to hearts with right ventricular hypertrophy (RVH) and found significantly different motion metrics from those of normal hearts. In particular, a lessened strain angle and minimum principal strain was found in RVH hearts[10]. There was also an observed "twisting" of the RV with respect to the LV which would make an LV-centric system useful to analyze the RV-LV interactions. While notable, this local strain information does not connect back to the organ-level changes that we are concerned with such as axial contraction and peristaltic motion.

3.3 Shape Representation using NURBS [3]

An additional project completed by researchers at Zhejiang University of Technology is particularly insightful for our later step of shape representation, which will be thoroughly described within Section 5.1. In the work done by Chen and Guan [3], they propose a method for representing the total cardiac surface in terms of NURBS (Nonuniform rational B-splines). Using cardiac MRI images (with no temporal component), they directly obtain their point cloud by fitting an ASM (active shape model) directly to the image volume to obtain a triangular mesh then convert that to a tetrahedral mesh and fit it to a NURBS geometry. Since it is not over any time span, the approach

shows a proof of concept that shows that measures of volume can be quite accurately measured from this method. Unfortunately, the paper does not go into great detail about the fitting process, but it once again brings up the issue of a coordinate system that is geometrically valid without incorporating important structural features. By pairing aspects of this approach with the proposed method pipeline (as detailed in the following chapter) and extending it to a temporal data set, we hope to derive more organ-level motion metrics. In fact, the paper even goes into detail of possible extensions to images over the cardiac cycle, but does not derive any kinematic metrics (outside of volume change over time).

Chapter 4

Data Processing Pipeline

In order to process clinical imaging data for analysis, a computational framework has been developed as a project by the Center for Cardiovascular Simulation at UT Austin. In this chapter, we detail each step of the current state of the pipeline and next steps. Further, the we will show these steps (listed in Figure 4.1) can lead to an improved representation of right ventricular shape and motion. The last two steps of NURBS representation and deformation analysis will be explored in more detail in Chapter 5.

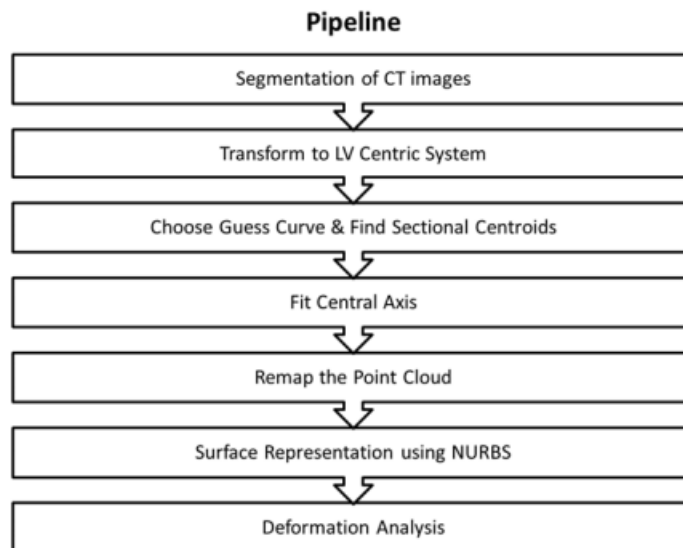


Figure 4.1: Data processing pipeline for analyzing cardiac CT images

In order to create physiologically-relevant metrics, this process focuses on remapping the geometry of the right ventricle with regards to a physiologically relevant central axis rather than an arbitrary system. While the central axis is not a physical structure within the heart, it represents the direction of the blood flow through the ventricle which governs all of its movement across the cardiac cycle.

4.1 Clinical Data

The raw data consists of bi-ventricular computed tomography (CT) images from the 1999 Dallas Heart Study (DHS) via the Dept. of Radiology at University of Texas Southwestern Medical Center at Dallas [CITE]. The DHS is a particularly good source for these analyses (and moving forward) as it was a multi-ethnic, population-based probability sample of Dallas County and has a variety of imaging data per patient. In this report, we only examined CT data where for a single heart, five images were obtained at intervals starting from end-diastole to mid-systole. From each image, the right ventricle was isolated and then segmented using anatomical features as a guide in order to produce a point cloud as our starting data points.

4.2 Determining End Planes

For a given sample, there is now a point cloud $P(x, y, z)$ of discrete three-dimensional points which represents the heart's geometry at the given time point in the cardiac cycle. Next, in order to define the central axis, we need

to have "end planes" which define the fixed physical bounds of the geometry. The start/acute end plane corresponds to the RV free wall while the end/sinus end plane corresponds to the pulmonary valve on the other side. To determine the planes, three points (P_1, P_2, P_3) were manually marked and then the first approximation of the end plane was defined by (P_2, η) where η is the normal defined as $\eta = (P_1 - P_2) \times (P_3 - P_2)$. From there, to find the best-fit plane, the least squares matrix is defined as $(P - X)^T \cdot (P - X)$ such that the centroid of the three points is $X = \frac{1}{N} \sum_{i=1}^N P_i$. Then, we can consider the principle eigenvector to be the normal to the best fit plane passing through X.

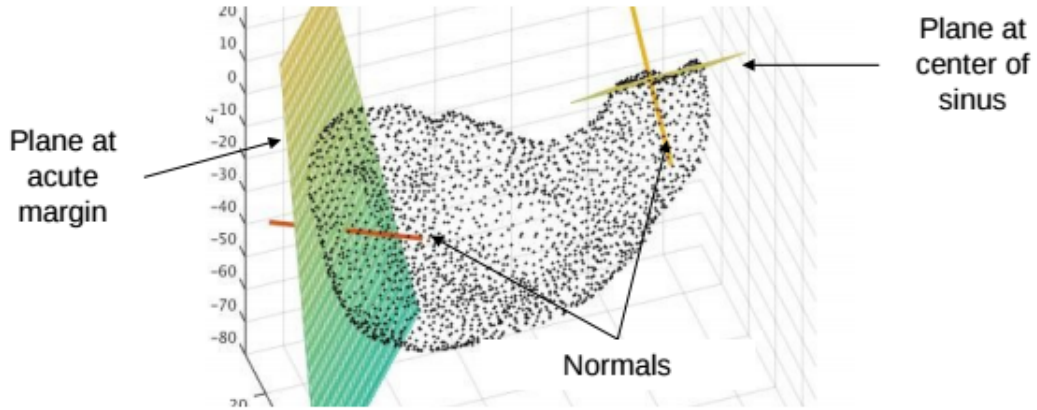


Figure 4.2: The two best-fit end planes and their respective normal vectors.

4.3 Determining the Central Axis

The central axis (CA) is the vital part of this pipeline as it ties the RV geometry to the hemodynamics of the cardiovascular system. Since the RV's primary function is pumping blood, the CA is designated by the path of blood

flow and allows us to re-map the geometry with respect to that flow path. For these purposes, a central axis needs to:

1. Pass through the end points
2. Pass through sectional centroids
3. Have a tangent parallel to the the two end normals

4.3.1 Sectional Centroids

For our first approximation of an ideal CA, a cubic bezier curve is used with four control points (P_0, P_1, P_2, P_3) where P_0 and P_3 are the two end points that we identified in Section 4.2. A bezier curve is used to maintain smoothness and easy shape manipulation to fit the given criteria. In order to find the appropriate values for the two internal control points, we use the third tangency condition to construct the following formulas:

$$B_1(t) = (1 - t)^2 P_0 + 3(1 - t)^2 t P_1 + 3(1 - t) t^2 P_2 + t^3 P_3, \quad t \in \{0, 1\} \quad (4.1)$$

$$P_1 = \left[a, y_0 + \frac{n_0^y}{n_0^x} (a - x_0), z_0 + \frac{n_0^z}{n_0^x} (a - x_0) \right] \quad (4.2)$$

$$P_2 = \left[b, y_3 + \frac{n_3^y}{n_3^x} (b - x_3), z_3 + \frac{n_3^z}{n_3^x} (b - x_3) \right] \quad (4.3)$$

In terms of notation, n_0^x represents the x component of the normal for P_0 and so on. The components of P_i in each direction are written as x_i, y_i , and z_i with a and being free parameters to be solved.

The first central axis shown in Figure 4.3 now has well oriented normals and uses the end points so it fulfills the first and third requirements that we defined for a central axis. Now, in order to fulfill the second condition, it must pass through "sectional centroids" in order to accurately represent the center of the geometry along the entire axis. To do so, the total length of the geometry and it's axis are divided into equally spaced sections each denoted by $t_i = \frac{i}{s_{total}-1}$ where s_{total} = total number of sections (which was chosen to be 50).

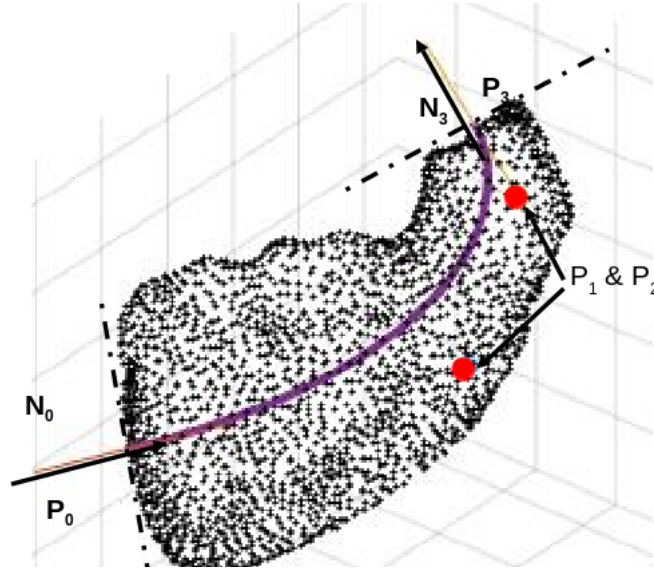


Figure 4.3: Bezier curve and its control points alongside the point cloud $P(x, y, z)$. Parameter values of $a=65$ and $b=59$ were used.

For each of these points t_i , we can now compute the true geometric centroid. However, since the point cloud is not very uniform, some subspaces are significantly more dense or sparse. In order to compensate for this, we first divide the point cloud into sections based on minimizing the perpendicular

distance from the nearest t_i on the initial curve. Then we can project the points onto the sectional plane in order to condense it to a two-dimension problem. This allows us to determine the convex hull to enclose the projected points and label the points that fall inside the threshold. By averaging the locations of the points in that area, we then obtain the centroid and can determine where it lies in the three-dimensional point cloud. Once we have done this for all sections, we not have a list of s_{total} sectional centroids (and associated planes) that the curve should adhere to.

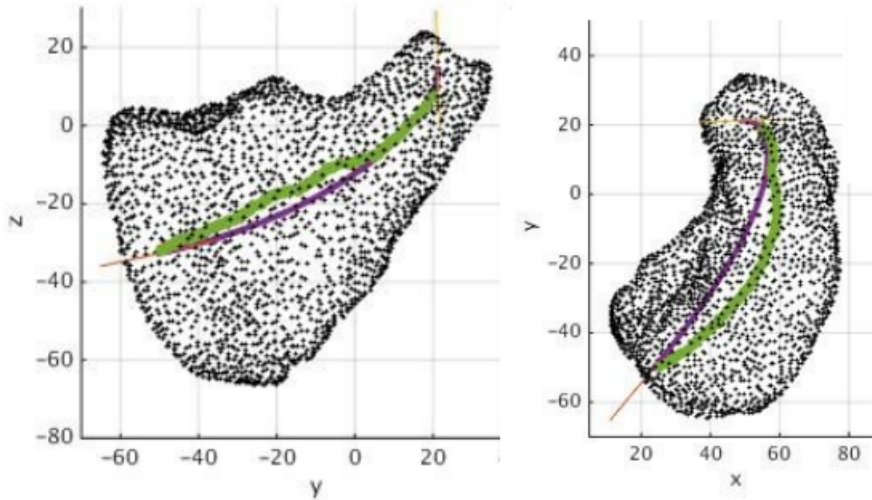


Figure 4.4: The right ventricle point cloud with the initial bezier curve (purple), the sectional centroids (green), and two end normals (yellow)

4.3.2 Second Bezier Curve

As expected, in Fig. 4.4, it is clear that our initial guess curve does not fulfill the requirement of passing through all (or even most) of the sectional centroid so we must adapt it. Let us define our sectional centroids to be

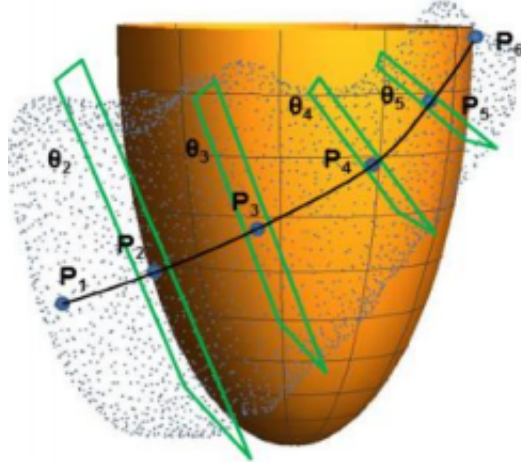


Figure 4.5: Central axis and sectional centroids (and corresponding sectional planes).

$I_i, i = \{0, 1, \dots, s_{total} - 1\}$ and construct a new bezier curve with four control points (P_0, P_1, P_2, P_3) as:

$$B_2(t) = (1 - t)^2 P_0 + 3(1 - t)^2 t P_1 + 3(1 - t)^2 t^2 P_2 + t^3 P_3 \quad (4.4)$$

Now, we need to be fit the curve to our sectional centroids by minimizing the cost function $e = \sum_{i=0}^{s_{total}-1} \|B_2(t_i) - I_i\|^2$. However, since our bezier curve is defined in terms of t_i , we need to find the corresponding sectional centroid I_i . By assessing the proportion of the chord length between two consecutive sectional centroids (defined in Eq. 4.5) over the total length, we can define t_i in terms of sectional centroid indices. This allows us to rewrite our cost function as Equation 4.6.

$$\ell_j = \|I_j - I_{j-1}\| \quad (4.5)$$

$$e(a, b) = \sum_{i=0}^{s_{total}-1} \|B_2(t_i, a, b) - I_i\|^2 \quad , \quad t_i = \frac{\sum_{j=0}^i \ell_j}{\sum_{j=0}^{s_{total}-1} \ell_j} \quad (4.6)$$

Similar to our first bezier curve, the end points are fixed as our first and last control points. However, to solve for the internal control points, we can now simply minimize the cost function by setting $\frac{\partial e}{\partial a}$ and $\frac{\partial e}{\partial b}$ both to zero. This gives us the appropriate parameters ($a = 31.106$, $b = 81.18$) for Equations 4.2 and 4.3 which solves for the two internal control points P_1 and P_2 respectively. With all four control points fit and B_2 defined, we now have a curve that passes through sectional centroids while still maintain the required properties of our initial curve.

4.4 Remapping

With a central axis that now fulfills all the geometric and fit conditions, we want to transform the coordinate system continuously with respect to this central axis. In order to perform the re-mapping, we use a Frenet-Serret frame, which is a locally defined system on a continuous curve consisting of a orthonormal basis of three components: a tangent to the curve (T), normal unit vector (N), and bi-normal (V) as product of T and N shown below.

$$T(t) = \frac{B'(t)}{\|B'(t)\|} \quad (4.7)$$

$$N(t) = \frac{T'(t)}{\|T'(t)\|} = \frac{B'(t) \times (B''(t) \times B'(t))}{\|B'(t)\| \|B''(t) \times B'(t)\|} \quad (4.8)$$

$$V(t) = T \times N = \frac{B'(t) \times B''(t)}{\|B'(t) \times B''(t)\|} \quad (4.9)$$

In order to determine which points of the RV data are considering to be on the frame at a point t , it must satisfy $T(t).(P(x, y, z) - B(t)) < \epsilon$ where ϵ is some planar tolerance. We must also compute the CA curve length s and a set of new local coordinates (x, y) for each point along the central axis. Using a Frenet frame, x and y are simply projections of a given point $P(x, y, z)$ onto the normal (N) and bi-normal(V) vectors respectively.

$$s_{curve} = \int_0^{t_i} \sqrt{B'(t).B'(t)}dt, \quad x = R.N, \quad y = R.V \quad (4.10)$$

Figure 4.6 below shows the results of final mapping of a normal human right ventricle from two different perspectives. As you can see, the central axis is now "straightened out" and the point cloud has been re-oriented.

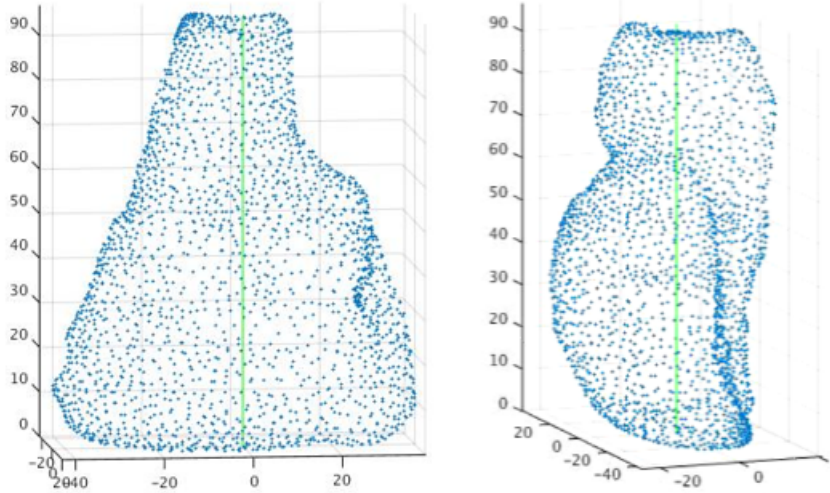


Figure 4.6: The re-mapped point clouds with the central axis shown in green.

Chapter 5

Preliminary Deformation Analysis

As previously discussed in Chapter 2, work by Chen and Guan showed the potential for using deformable NURBS as parametric shape representation for the heart. While that project primarily focused on volume and associated metrics, we will explain how this could also be applied to deformation analysis across time. In this section, we will provide an overview of using NURBS and some exploratory 2-D analysis of our remapped point clouds. Further, we will discuss how this will be extended to three-dimensional analysis as well.

5.1 NURBS

Non-uniform rational basis splines (NURBS) have become a common mathematical model to represent complex geometric shapes for isogeometric analysis and computer graphics. Most notably, computer-aided design (CAD) systems use NURBS geometries as their underlying parametric surfaces to represent and modify physical systems for engineering and data visualization [33].

Using a NURBS-based framework allows one to represent both analytical shapes and the irregular free-form shapes that are more often encountered

in biological systems. Further, they are invariant under projection and affine transformations with regards to scale, rotation, and shear which makes it quite ideal for kinematic analysis and manipulation [22]. Additionally, they hold a strong convex hull property meaning it is contained within the convex hull of its control points [4]. While for complex data such as cardiac images, NURBS can be a good solution, it is not as efficient for more traditional shapes such as a perfect circle (which requires ten knots and seven control points rather than just the center and radius).

5.1.1 Definition

A NURBS curve in two dimensions can be mathematically defined as a piecewise rational polynomial function composed of various weighted basis functions and is of the form

$$C(u) = \frac{\sum_{i=0}^n N_i(u)w_i P_i}{\sum_{i=1}^n N_i(u)w_i} \quad (5.1)$$

where n is the total number of control points, P_i is the i th control point, $N_i(u)$ is the i th b-spline basis function formed by the knot vector u , and w_i is the associated weight.

Similarly, we can define a NURBS surface in three dimensions by generalizing the tensor product surface form [22] to derive equation 5.2. Similar to Eq. 5.1, w and P represent the weights and control points respectively (but is referred to as a control net in two dimensions). The B-splines in each respective direction are separated as $N(u)$ and $N(v)$ as functions of the two knot vectors u and v .

$$S(u, v) = \frac{\sum_{i=0}^n \sum_{j=1}^m N_{i,p}(u) N_{j,q} w_{i,j} P_{i,j}}{\sum_{i=0}^n \sum_{j=1}^m N_{i,p}(u) N_{j,q} w_{i,j}} \quad (5.2)$$

In order to specify a NURBS geometry, we must choose a set of control points and a knot vector. For a given NURBS curve of degree N , there must be at least $N + 1$ control points with each having some associated weight. Secondly, the knot vector needs to consist of exactly $(\text{degree}-1+C)$ numbers where C is the number of control points [23].

A NURBS curve can be constructed from a set of discrete data points (such as a point cloud) via data fitting, interpolation, or manual selection [22]. Using a least-squares fit approach and given an initial set of data points $Q_k, k = 0 \dots n$, we need to find some b-spline curve N_i that fulfills Eq. 5.3 for some parameters u_k

$$Q_k = C(u_k) = \sum_{i=0}^n P_i N_{i,p}(u_k) \quad (5.3)$$

Defining this in matrix form as $Q = NP$ and then using the fact that the system is overdetermined (since there are more data points than control points), we can use the following equation to approximate the data with Q^* in Eq. 5.4. Starting with some initial parameter guess, we can assess the least squares error and modify the parameters until it converges within a certain error tolerance [23]. Similarly, we can extend the same approach for NURBS surfaces.

$$Q^* = (N^T N)^{-1} N^T P \quad (5.4)$$

5.1.2 Deformation

Since NURBS is a piecewise function of low degree polynomials, one of the crucial properties is that local deformation of the shape only has a local effect within that interval of basis functions while maintaining the global shape [4]. The shape of a NURBS geometry can be changed easily via changing the weights or modifying the control point(s) as well as knot vector changes or just changing the initial data points then re-constructing it [27]. The former two techniques are shown in Fig. 5.1 below on an example curve.

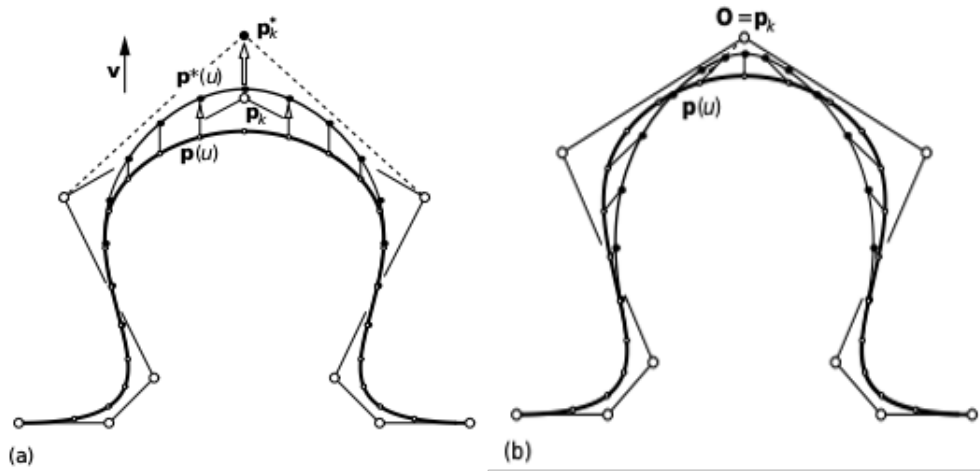


Figure 5.1: The two main methods of modifying a NURBS curve.
 (a) The effect of displacing control point p_k to p_k^* along direction v by a distance d . This produces a new curve $p^*(u)$ which is partially shifted towards v .
 (b) The result of assigning a new weight w_k^* to the k -th control point. The origin O of the coordinate system is set to control point p_k . Images from [27].

While the examples above represent a simplistic push/pull on their own, these approaches can be systematically used to characterize a specific deformation mode from our starting geometry which could be used to describe

aspects of complex motion such as the bending, contractile, and peristaltic movement in Fig. 5.3.

5.2 Application

In order to apply these methods to our remapped three-dimensional point clouds, we used the simpler case of using NURBS curves over a 2-D surface as a proof of concept and hope to extend it. As seen below from the remapped geometries, some clear trends are already noticeable with a very asymmetric deformation pattern.

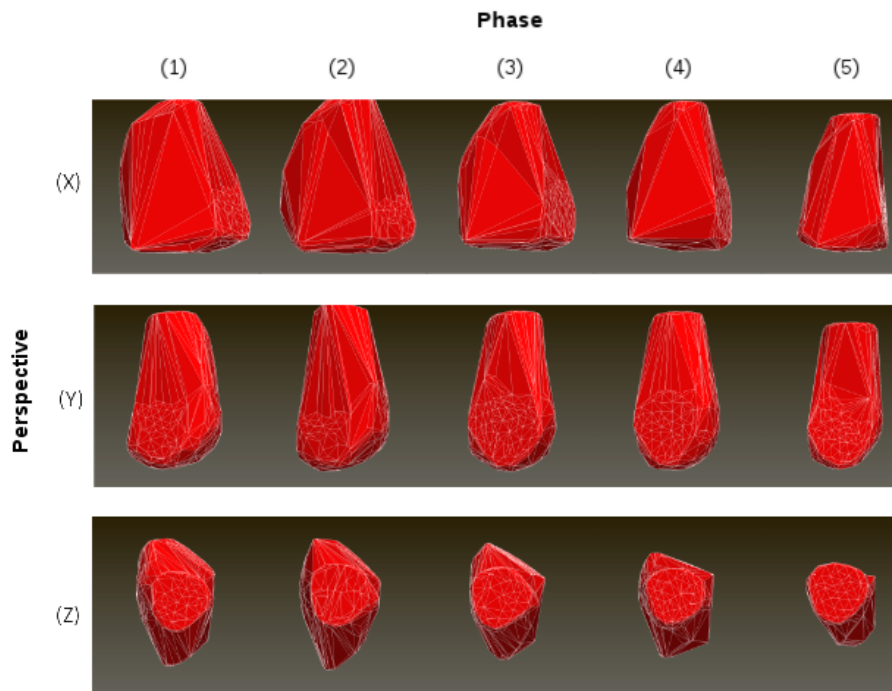


Figure 5.2: The re-mapped point clouds over time from three perspectives.

Phase:	1	2	3	4	5
X-axis length	75.6488	80.9228	72.2077	64.9070	55.3044
Y-axis length	53.6094	54.3632	51.7027	49.1525	46.7785
Z-axis length	97.7163	98.4612	96.8521	96.3695	91.2548

Table 5.1: Relative axes length over the five phase points for one normal RV.

Although we have not developed the 3-D analysis, Figure 5.3 shows some of the main deformation motions that we expect to be able to decompose it's motion into. During each stage in the cardiac cycle, we hope to be able to see a different configuration of motions such as these with some becoming more pronounced during diastole or systole. Many of these motions involve stretching or contracting along the direction of the central axis or twisting from either of the end planes.

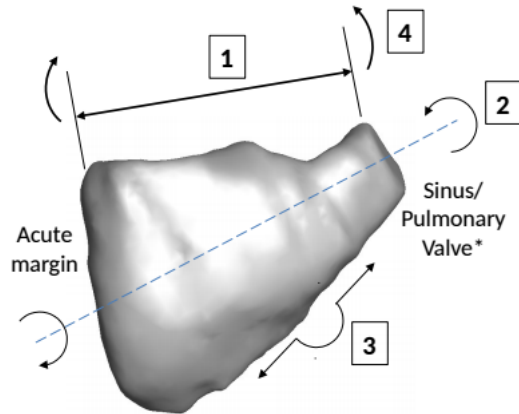


Figure 5.3: Four main types of motion expected to make up RV kinematics.

- (1) Elongation and contraction.
- (2) Twisting and rinsing.
- (3) Peristaltic movement.
- (4) Bending.

Chapter 6

Conclusion and Future Work

In this report, we showed that the right ventricle is still poorly understood in some respects despite playing an essential role in the cardiac system and associated diseases. We introduced some of the underlying methods to build a pipeline for creating a physiologically meaningful representation of the right ventricle and showed how it can be potentially used to analyze the motion throughout the cardiac cycle.

The next step of this project would be to extend our kinematic analysis to three dimensions by using a trivariate NURBS representation and developing a method to extract the relative deformation gradient tensor and strain between time points. In addition, the entire pipeline and deformation measures would need to be rigorously validated using more in-vivo data from the DHS data set. Once we know we have a valid and physiologically-accurate framework, we would like to compare the deformation and motion between hearts with and without pulmonary hypertension (PH).

Ultimately, this would allow us to understand cardiovascular diseases better and what role the RV plays in it. This could potentially aid in treatment when paired with a predictive model or diagnostics if applied to image

processing and classification.

Bibliography

- [1] Emelia J. Benjamin. Heart disease and stroke statistics—2017 update: A report from the american heart association. *Circulation*, 2017.
- [2] Michael J. Borden, Michael A. Scott, John A. Evans, and Thomas J. R. Hughes. Isogeometric finite element data structures based on bzier extraction of nurbs. *International Journal for Numerical Methods in Engineering*, 87(1-5):15–47, 2011.
- [3] S. Y. Chen and Q. Guan. Parametric shape representation by a deformable nurbs model for cardiac functional measurements. *IEEE Transactions on Biomedical Engineering*, 58(3):480–487, March 2011.
- [4] S. Cheng, X. Zhang, and K. Tang. Shape modification of b-spline curve with geometric constraints. In *2007 International Conference on Computational Intelligence and Security (CIS 2007)*, pages 325–329, Dec 2007.
- [5] G. E. D’Alonzo, R. J. Barst, S. M. Ayres, E. H. Bergofsky, B. H. Brundage, K. M. Detre, A. P. Fishman, R. M. Goldring, B. M. Groves, and J. T. Kernis. Survival in patients with primary pulmonary hypertension. Results from a national prospective registry. *Ann. Intern. Med.*, 115(5):343–349, Sep 1991.

- [6] A. F. Frangi, D. Rueckert, J. A. Schnabel, and W. J. Niessen. Automatic construction of multiple-object three-dimensional statistical shape models: application to cardiac modeling. *IEEE Transactions on Medical Imaging*, 21(9):1151–1166, Sept 2002.
- [7] M. G. George, L. J. Schieb, C. Ayala, A. Talwalkar, and S. Levant. Pulmonary hypertension surveillance: United States, 2001 to 2010. *Chest*, 146(2):476–495, Aug 2014.
- [8] D.A. Goor and C.W. Lillehei. *Congenital Malformations of the Heart: Embryology, Anatomy, and Operative Considerations*. Grune & Stratton, 1975.
- [9] C. R. Greyson. Pathophysiology of right ventricular failure. *Crit. Care Med.*, 36(1 Suppl):57–65, Jan 2008.
- [10] I. Haber, Dimitris N. Metaxas, and Leon Axel. Three-dimensional motion reconstruction and analysis of the right ventricle using tagged {MRI}. *Medical Image Analysis*, 4(4):335 – 355, 2000.
- [11] François Haddad, Sharon A. Hunt, David N. Rosenthal, and Daniel J. Murphy. Right ventricular function in cardiovascular disease, part i. *Circulation*, 117(11):1436–1448, 2008.
- [12] S. Y. Ho and P. Nihoyannopoulos. Anatomy, echocardiography, and normal right ventricular dimensions. *Heart*, 92 Suppl 1:2–13, Apr 2006.
- [13] J.W. Hurst. *Atlas of the Heart*. McGraw-Hill, 1988.

- [14] Nallig Leal, Esmeide Leal, and John William Branch. *Simple Method for Constructing NURBS Surfaces from Unorganized Points*, pages 161–175. Springer Berlin Heidelberg, Berlin, Heidelberg, 2010.
- [15] P. J. Leary, C. E. Kurtz, C. L. Hough, M. P. Waiss, D. D. Ralph, and F. H. Sheehan. Three-dimensional analysis of right ventricular shape and function in pulmonary hypertension. *Pulm Circ*, 2(1):34–40, 2012.
- [16] M. J. Ledesma-Carbayo, J. Kybic, M. Desco, A. Santos, M. Suhling, P. Hunziker, and M. Unser. Spatio-temporal nonrigid registration for ultrasound cardiac motion estimation. *IEEE Transactions on Medical Imaging*, 24(9):1113–1126, Sept 2005.
- [17] C. H. Lorenz, E. S. Walker, V. L. Morgan, S. S. Klein, and T. P. Graham. Normal human right and left ventricular mass, systolic function, and gender differences by cine magnetic resonance imaging. *J Cardiovasc Magn Reson*, 1(1):7–21, 1999.
- [18] T. Makela, P. Clarysse, O. Sipila, N. Pauna, Quoc Cuong Pham, T. Katila, and I. E. Magnin. A review of cardiac image registration methods. *IEEE Transactions on Medical Imaging*, 21(9):1011–1021, Sept 2002.
- [19] Vinh Phu Nguyen, Pierre Kerfriden, Stéphane P. A. Bordas, and Timon Rabczuk. Isogeometric analysis suitable trivariate nurbs representation of composite panels with a new offset algorithm. *Comput. Aided Des.*, 55:49–63, October 2014.

- [20] Sangkun Park and Kunwoo Lee. High-dimensional trivariate nurbs representation for analyzing and visualizing fluid flow data. *Computers Graphics*, 21(4):473 – 482, 1997.
- [21] Diletta Peluso, Francesco Tona, Denisa Muraru, Gabriella Romeo, Umberto Cucchini, Martina Perazzolo Marra, Sabino Iliceto, and Luigi Paolo Badano. Right ventricular geometry and function in pulmonary hypertension: Non-invasive evaluation. *Diseases*, 2(3):274–295, 2014.
- [22] L. Piegl. On nurbs: a survey. *IEEE Computer Graphics and Applications*, 11(1):55–71, Jan 1991.
- [23] Les A. Piegl and Wayne Tiller. Computing offsets of {NURBS} curves and surfaces1. *Computer-Aided Design*, 31(2):147 – 156, 1999.
- [24] Lisa J Rose-Jones and Vallerie V Mclaughlin. Pulmonary hypertension: Types and treatments. *Current Cardiology Reviews*, 11.1:73–79, 2015.
- [25] Rich S, Dantzker Dr, Ayres Sm, and et al. Primary pulmonary hypertension: A national prospective study. *Annals of Internal Medicine*, 107(2):216–223, 1987.
- [26] M. S. Sacks, C. J. Chuong, G. H. Templeton, and R. Peshock. In vivo 3-d reconstruction and geometric characterization of the right ventricular free wall. *Annals of Biomedical Engineering*, 21(3):263–275, 1993.
- [27] J. Sanchez-Reyes. A simple technique for nurbs shape modification. *IEEE Computer Graphics and Applications*, 17(1):52–59, Jan 1997.

- [28] W. P. Segars, D. S. Lalush, and B. M. W. Tsui. A realistic spline-based dynamic heart phantom. *IEEE Transactions on Nuclear Science*, 46(3):503–506, Jun 1999.
- [29] James A. Shaver, Richard A. Nadolny, James D. O’Toole, Mark E. Thompson, P. S. Reddy, Donald F. Leon, and Edward I. Curtiss. Sound pressure correlates of the second heart sound. *Circulation*, 49(2):316–325, 1974.
- [30] Florence Sheehan and Andrew Redington. The right ventricle: anatomy, physiology and clinical imaging. *Heart*, 94(11):1510–1515, 2008.
- [31] Arthur E Weyman. Principles and practice of echocardiography. 1994.
- [32] Jia Wu, Yingqian Wang, Marc A Simon, and John C Brigham. A new approach to kinematic feature extraction from the human right ventricle for classification of hypertension: a feasibility study. *Physics in Medicine and Biology*, 57(23):7905, 2012.
- [33] Gang Xu, Bernard Mourrain, André Galligo, and Timon Rabczuk. High-quality construction of analysis-suitable trivariate NURBS solids by reparameterization methods. *Computational Mechanics*, 54(5):1303–1313, November 2014.

Vita

Rose Janet Simmons received her Bachelor of Science in Computer Science from The University of Texas at Austin. During her time at UT Austin, she completed summer internships at J.P. Morgan, John Hopkins Center for Talented Youth in Hong Kong, Applied Research Laboratories and Square, Inc. Additionally, she worked in various roles at UT during the school year as a UTeach after-school instructor, teaching assistant, peer mentor, and finally a graduate research assistant on the Project 2021 initiative in her last year. Following graduation, Rose is moving to San Francisco, California where she will be working as a software engineer at Square. To contact Rose directly, email her at rsimmons@utexas.edu

This report was typeset with \LaTeX^\dagger by the author.

[†] \LaTeX is a document preparation system developed by Leslie Lamport as a special version of Donald Knuth's \TeX Program.